Earth and Planetary Science Letters, 57 (1982) 377–397
Elsevier Scientific Publishing Company, Amsterdam – Printed in The Netherlands

[2]

Seismicity, normal faulting, and the geomorphological development of the Gulf of Corinth (Greece): the Corinth earthquakes of February and March 1981

J.A. Jackson [1], J. Gagnepain [2], G. Houseman [1], G.C.P. King [1], P. Papadimitriou [2], C. Soufleris [1] and J. Virieux [2]

[1] *Bullard Laboratories, Madingley Rise, Madingley Road, Cambridge, CB3 0EZ (U.K.)*
[2] *Institut de Physique du Globe, L.E.G.S.P., Université Pierre et Marie Curie, 4, place Jussieu, 75230 Paris Cedex 05 (France)*

Received August 25, 1981
Revised version received November 2, 1981

Three major destructive earthquakes of M_s 6.7, 6.4, 6.4 occurred in the eastern part of the Gulf of Corinth in February and March 1981. Associated normal faulting was observed on both the north and the south sides of the Gulf. Examination of teleseismic, local seismic, surface faulting and geomorphological data suggests that the first and second of these shocks activated major north-dipping normal faults. These faults control the topography and bathymetry and are related to the recent uplift and subsidence of the coastline. It is probable that the first earthquake occurred on a fault which outcrops underwater and the second on a fault which is visible on land. It appears that the third shock activated an antithetic normal fault dipping southwards on the north side of the Gulf and that the overall structure of the Gulf of Corinth graben is asymmetric. The northern antithetic fault clearly demonstrates the geomorphological changes associated with developing young normal faulting. In addition, we suggest that observations of recent coastline movement provide a powerful tool for identifying major active fault systems and predicting their historical role in the paleogeography of an area.

1. Introduction

On February 24, 25 and March, 4, 1981, three major earthquakes of magnitudes M_s 6.7, 6.4, 6.4 (U.S.G.S.) occurred in the easternmost part of the Gulf of Corinth (Fig. 1 and Table 1). Associated normal faulting appeared on land on both the north and south sides of the Gulf. A clear eastwards migration of seismicity is evident in both the U.S.G.S. and relocated epicentres as well as the surface faulting; which, in the north, appeared only after the shock of March 4.

The Gulf of Corinth has long been recognised as a graben structure formed by normal faulting. Major earthquakes are common, and the last important one that also affected the town of Corinth occurred in 1928 [1,2]. Unfortunately, helpful field accounts of the surface deformation associated with Gulf of Corinth events are rare. Richter [3] attributes the surface effects of the 1861 earthquake in the western part of the Gulf to normal faulting and McKenzie [4] shows two teleseismic fault plane solutions in the area which also indicate normal faulting. Neotectonic studies [5–7] suggest that extension by normal faulting has been the dominant mode of deformation over most of eastern Greece and the Aegean since the Upper Miocene.

By March 4, 1981, a network of local seismographs from the Universities of Cambridge, Paris and Thessaloniki was set up in the area, and for a period of five weeks operated in conjunction with studies of surface faulting and shoreline changes. A combination of this field data with teleseismic

0012-821X/82/0000–0000/$02.75

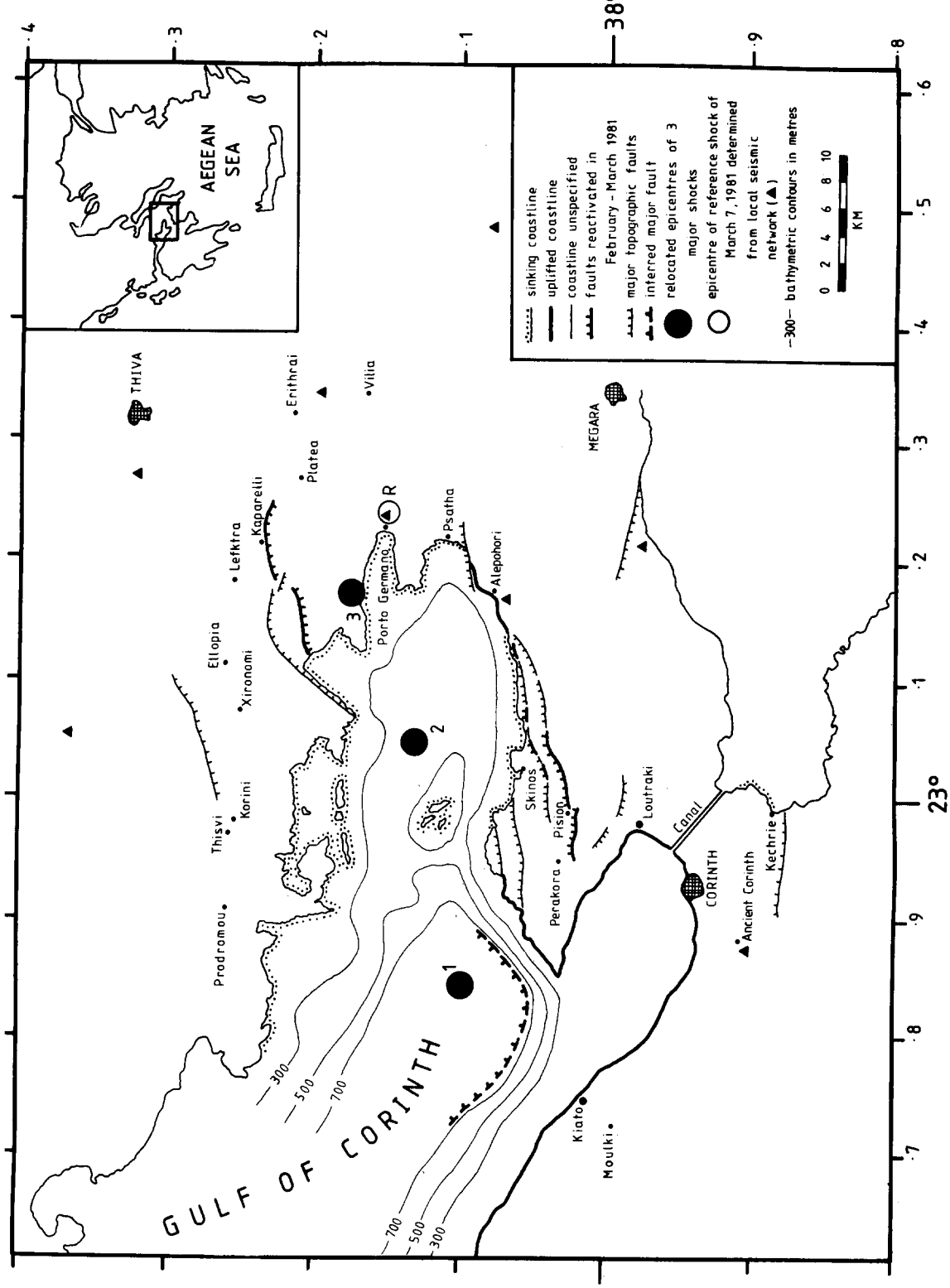

Fig. 1. Location and summary map. Epicentres of the February 24 (*1*), 25 (*2*), and March 4 (*3*) shocks are those relocated relative to *3* and placed geographically using the local epicentre determination for *R*, which was also located relative to *3*. Inset shows the area of this map.

TABLE 1

Hypocentral parameters of the three main shocks and the reference shock of March 7. Epicentres are from the relocations described in the text, and depths are from teleseismic waveforms for the first three shocks and from local seismic stations for March 7

Date	Origin time (GMT)	m_b	M_s	$M_0 \times 10^{25}$ (dyne cm)	Lat., long.	Depth (km)	Number of stations in relocation
February 24, 1981	20 53 38.7	5.9	6.7	7.28	38.099, 22.842	10	120
February 25, 1981	02 35 53.3	5.5	6.4	1.68	38.135, 23.050	8	108
March 4, 1981	21 58 07.3	5.9	6.4	0.97	38.176, 23.170	8	–
March 7, 1981	11 34 43.8	5.5	–	–	38.156, 23.241	11	58

observations provided an opportunity to study the three-dimensional evolution of an active graben. Relations between the deformation at the surface and that at depth were not immediately obvious in this 1981 earthquake sequence, and it is the aim of this paper to demonstrate the usefulness of differing types of data in understanding complex problems of structural geology. For this reason the necessary observations are discussed before any interpretations are given.

2. Faulting on the south side of the Gulf

Fresh surface faulting extending for 12–15 km appeared on the south side of the Gulf during the night of February 24 and 25 when the first two major shocks occurred at 10:53 p.m. and 04:35 a.m. local time. Severe damage was inflicted on the predominantly stone housing in Perakora, Pision and Skinos (Figs. 2 and 3) but most of the clearest surface ruptures were away from these communities and did not cross roads or paths which were used in the time between the two shocks. Thus, in spite of extensive interviews with the local population, it was not possible to reliably determine, from first hand reports, how much of the faulting was attributable to each shock. Later, we conclude that most of the faulting on land was due to the second shock and that the first earthquake occurred on an offshore fault.

Fig. 2 shows the fresh surface faulting and includes representative slip (displacement) vectors measured at the surface. Fig. 3 shows the very marked relation between the east-west faulting and the topography. The main surface breaks begin about 2 km west of Pision and follow a very prominent high escarpment (at about the 600-m contour) eastwards through dense forest for about 10 km. Except for a region immediately south of Pision (Fig. 3) this fresh fault scarp is continuous, with only minor splay faults leading from it. Displacements reach 150 cm but are more typically in the range 50–70 cm and most slip azimuths are approximately due north. The entire section is clearly a reactivation of a fault in crystalline limestone which is responsible for the topography (Fig. 4). The new fault break often outcrops at the edge of alluvium or angular scree derived from the high limestone cliff of the fault face, and as a consequence slip vectors were sometimes difficult to measure. Only reliable slip observations are shown in Fig. 2. At the eastern end of this section the surface breaks are more discontinuous and outcrop at lower altitudes as they follow a more northerly trend down to another limestone escarpment which continues eastwards (Fig. 3). At the western end of the main section discontinuous ruptures cross the alluvial area south of Perakora, again with a more northerly trend. It is worth noting here, for later discussion, that at both ends of the main surface break section the ruptures become more fragmentary, with a more northerly trend and that also the slip vectors have less displacement with an azimuth more northeasterly in the western part and more northwesterly in the eastern part.

North of this section is another major fault

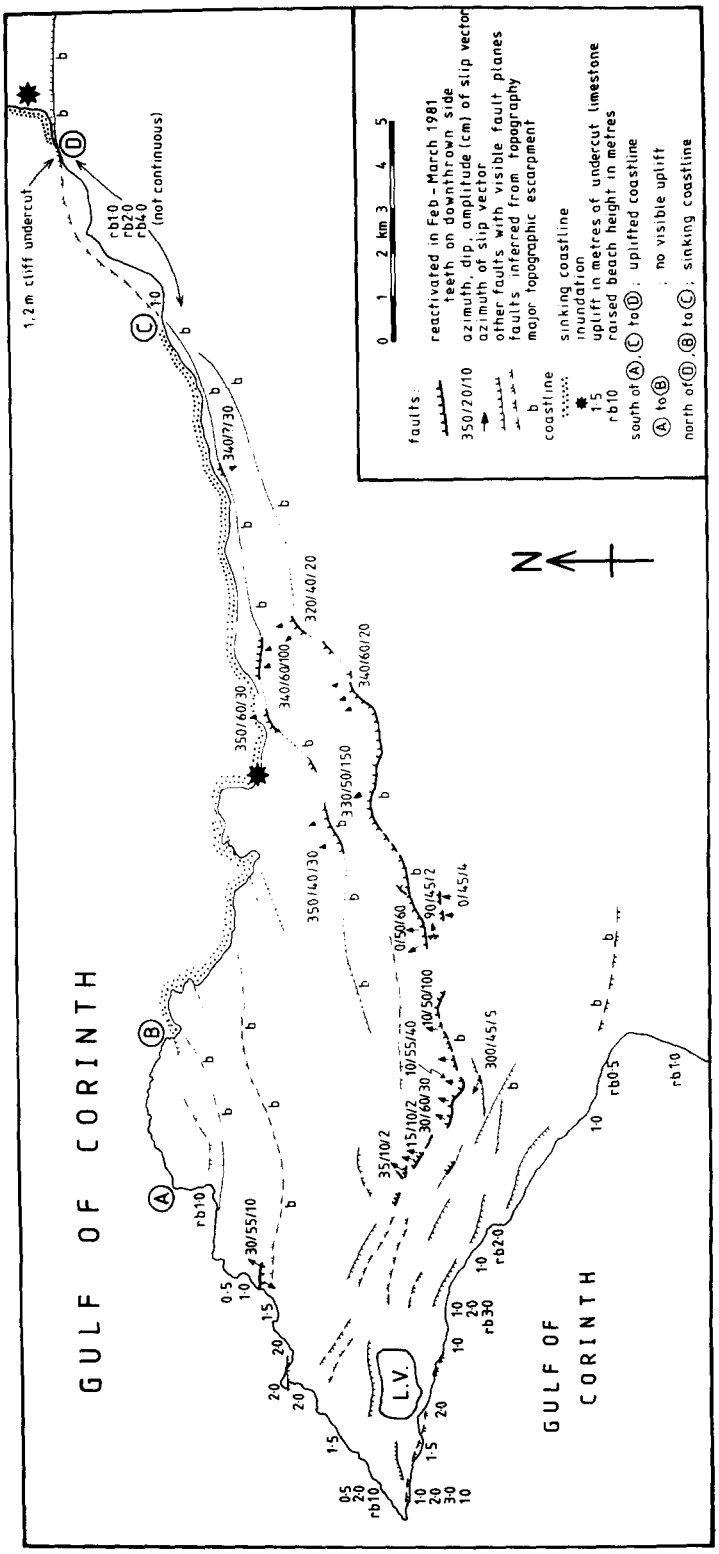

Fig. 2. Fault map of the southern shore of the eastern Gulf of Corinth, showing major and minor faults as well as 1981 surface breaks. Heavy lines with no teeth are open cracks.

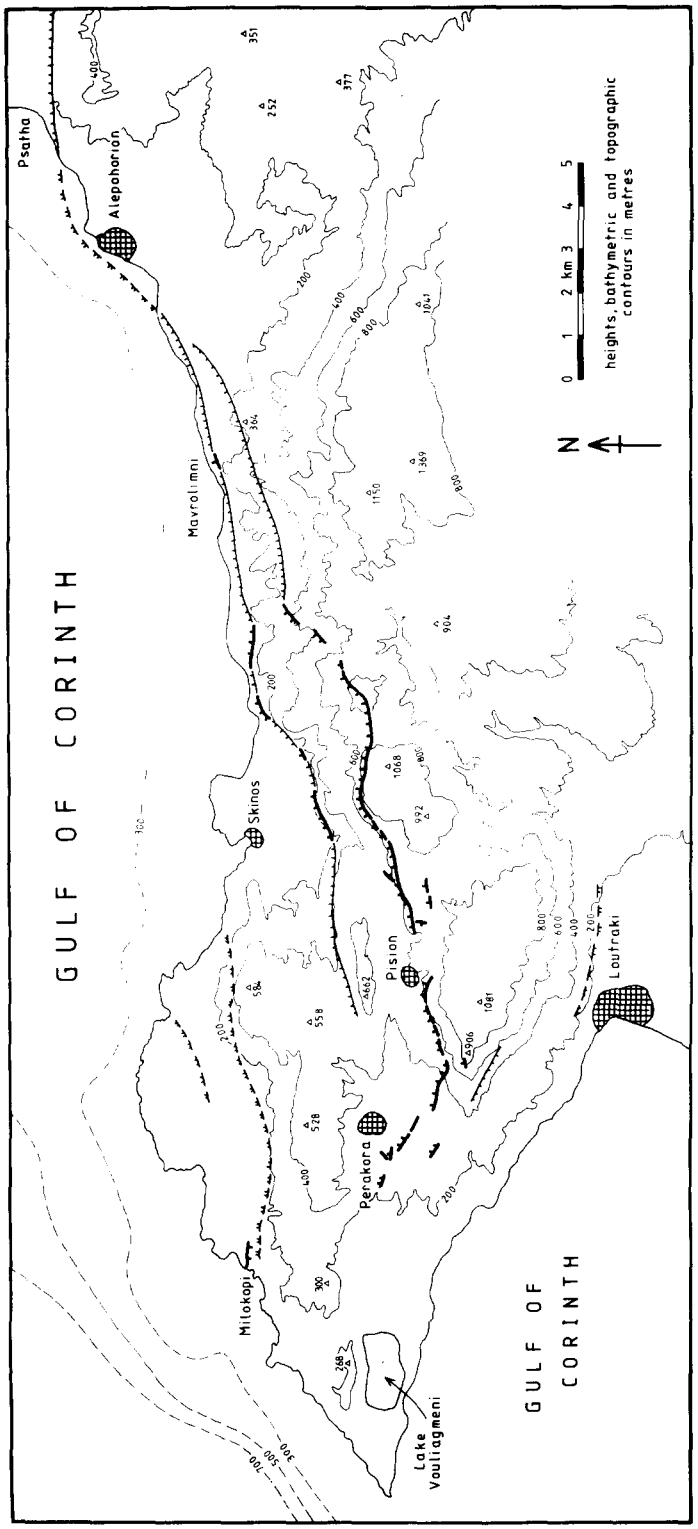

Fig. 3. Topographic map of the area in Fig. 2, showing only 1981 surface breaks (thick lines) and major fault escarpments.

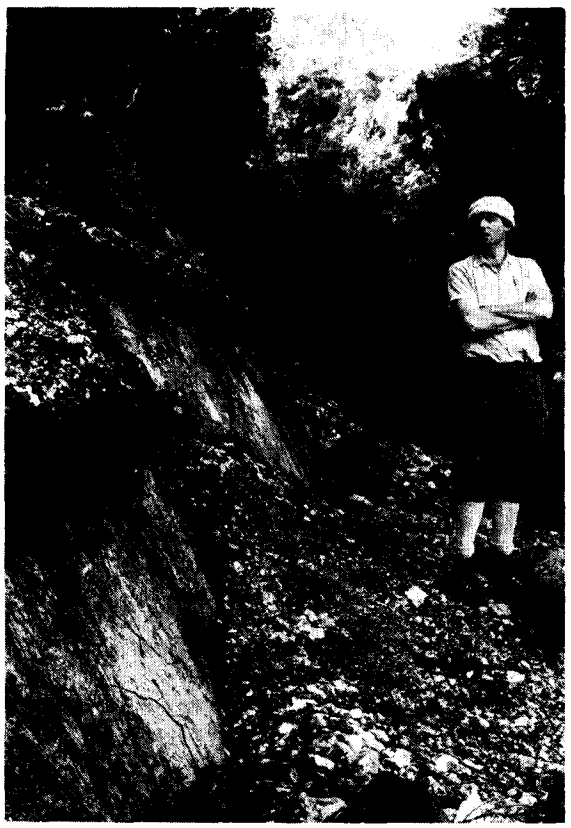

Fig. 4. The southern fault break 2 km east of Pision. A typical outcrop of the fault face against unconsolidated angular scree.

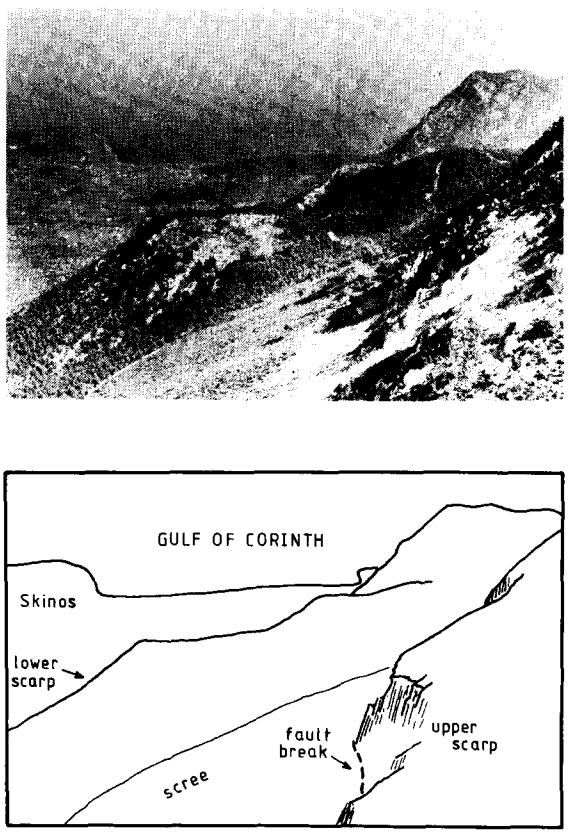

Fig. 5. View of the two main southern fault escarpments looking NE towards Skinos. The 1981 surface breaks were at the base of the cliff on the right. Note the large amount of angular scree.

escarpment which starts north of Pision and runs south of Skinos towards Alepohori (Figs. 2 and 3). Only small portions of this escarpment were reactivated, though it is clearly a major fault along its entire length. Where the fault outcrops at the edge of unconsolidated alluvium (at Mavrolimni and east of Skinos) widespread groundcracking suggests that some displacement at the surface may have been caused by shaking and ground instability rather than tectonic motion at depth. This is clearly the case in some places where anomalous slip vector directions vary rapidly over short distances.

These two fault escarpments are the dominant topographic features of this part of the southern shore and drop the surface from a height of 1100 m to sea level in two dramatic steps (Fig. 5). On the peninsular of Fig. 2 are numerous smaller faults which, individually, have a lesser influence on the topography. The majority shown are to the south or west of Perakora, but others are also present to the north. Of these, only a small section of a fault at Milokopi was found to be reactivated. These faults are all topographically less significant than the two major ones already discussed, though several of them (e.g. on the north side of Lake Vouliagmeni) show limestone fault surfaces up to 10 m high. The lack of significant fault scarps in the high ground immediately south of the main southern escarpment in Figs. 2 and 3 is real, though faulting downthrown to the south is evident near Loutraki.

3. Faulting on the north side of the Gulf

Normal faulting extending for 12 km with an east-west trend downthrown to the south appeared at the surface in the Livadostros valley on the north side of the Gulf after the shock of March 4. Interviews with the local population confirmed that these surface ruptures were not associated with the February 24 and 25 shocks.

Fig. 6 shows the detailed nature of the surface breaks and Fig. 7 shows their relation to the topography and to other faults. A prominent feature of this area is the Livadostros river, which drains a 300 m high, gently undulating, erosion surface by Platea. Southwest of Kaparelli the gentle topography is suddenly destroyed as the river forms a waterfall, enters a gorge, and rapidly changes height by about 200 m (Fig. 8). The surface breaks of March 4 consist of two continuous segments with fragmented ends. The first lies immediately south of Kaparelli, and forms a continuous scarp for about 5 km. It is clearly a reactivation of a pre-existing fault scarp about 3 m high which was easily visible before the earthquake (Fig. 9). Displacements on this segment average 50–70 cm with an azimuth of 030°N. At its eastern end the surface ruptures turn abruptly south on a splay fault and cross the alluvium of the valley floor (Fig. 10), and thus depart from the line of the old east-west scarp which continues eastwards but is not visibly reactivated at the surface. This change of trend is accompanied by a decrease in amplitude of displacement and a change to a more easterly slip azimuth. At the western end of this segment the surface ruptures follow the edge of the erosion surface alluvium until they turn abruptly south, and cross the gorge of the Livadostros river as a series of discontinuous cracks half a kilometre downstream of the waterfall. For 1.5 km south of the river the surface ruptures consist of a large number of small cracks and minor escarpments. In this region both northeasterly and northwesterly slip azimuths are found. Further west, a second, almost continuous, segment of 5 km length extends the faulting down to the coast. On this segment the average displacement is again 50–70 cm with an azimuth of 0–10°N; significantly different from that in the first segment. This second segment is again downthrown to the south and follows the next stream valley south of the Livadostros. The course of this stream is also clearly fault controlled, and its upstream (eastern) end appears as an anomalous longitudinal valley in the northsloping face of the ridge to the south (Fig. 7). Minor cracks and fissures were also found on the mountain south of Platea (Fig. 7), and on the southern slope of the ridge to the south of the western segment. In both places there is sufficient topography for gravitational effects to be possible, but the fissure alignments are improbable for landslippage and the slip vectors are consistent with those on the major fault segments. Minor cracks were also found immediately east of the waterfall where the river enters the gorge. These follow, in part, a prominent lineation visible on air photographs (Figs. 6, 8 and 11).

The dramatic change in level of the Livadostros river is the result of past motion on a large normal fault to the north of it. This forms a steep and high escarpment extending from the straight northwestern shore of Ormos Livadostros northwards to where it curves east, rapidly diminishing in height, onto the line of the reactivated fault south of Kaparelli. By dropping the land surface and river bed to the south, this fault has caused the Livadostros river to cut back into the old erosion surface, forming the gorge and waterfall. Evidence that the river valley above the gorge is also unstable is seen in terraces and minor nick-points (waterfalls; one at the easternmost end of the surface breaks and the other about 1 km upstream from Kaparelli), and is presumably the result of earlier motion on the fault segment south of Kaparelli.

Thus the March 4 surface ruptures are composed of two segments with a substantial offset. The eastern section cuts the old erosion surface in the upper Livadostros valley, but does not follow the western continuation of this fault. Instead, motion is transferred further south to a fault that has, as yet, only exerted a small influence on the topography. The variation of slip vector azimuths in the central section of discontinuous surface cracking is partly understandable as a necessary warping of the surface caused by the two offset fault segments (Fig. 12). The slip directions seen in

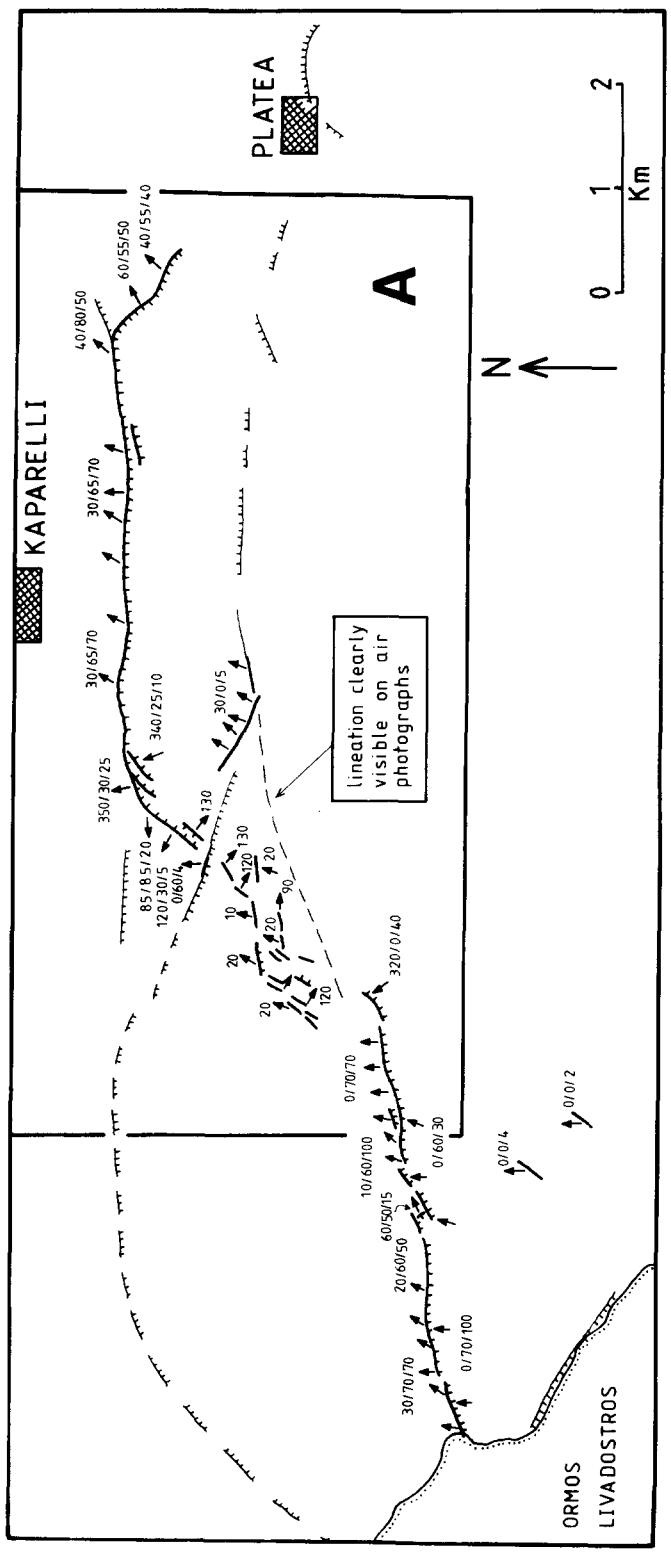

Fig. 6. Fault map of the northern surface breaks, with the same notation as Fig. 2. The area marked *A* is shown in the air photograph (Fig. 11). In the central area of discontinuous cracks and minor scarps only slip azimuths are shown. Displacements in this region are all small; mostly less than 10 cm.

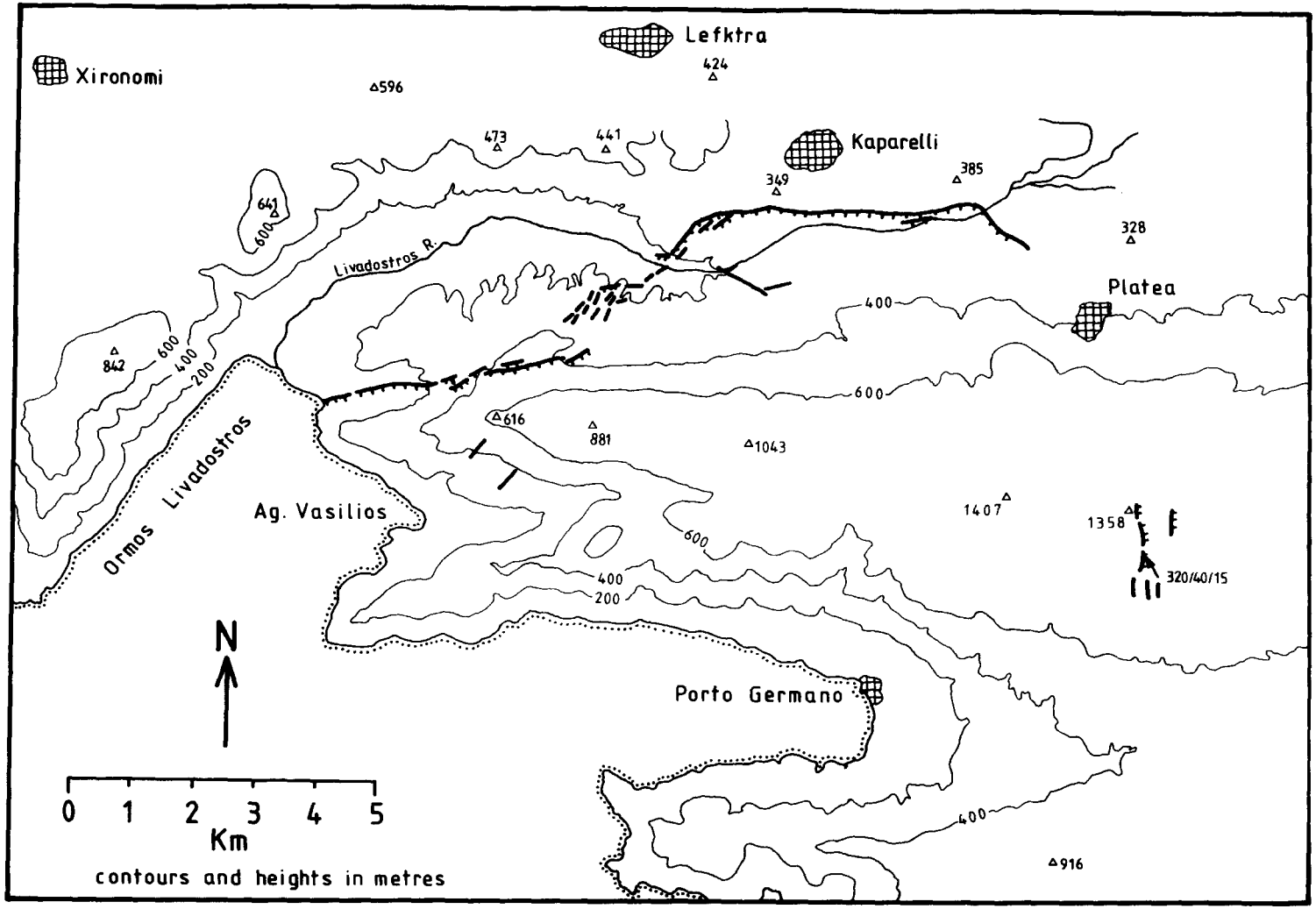

Fig. 7. Topographic map of the northern shore of the eastern Gulf of Corinth, showing only 1981 surface breaks.

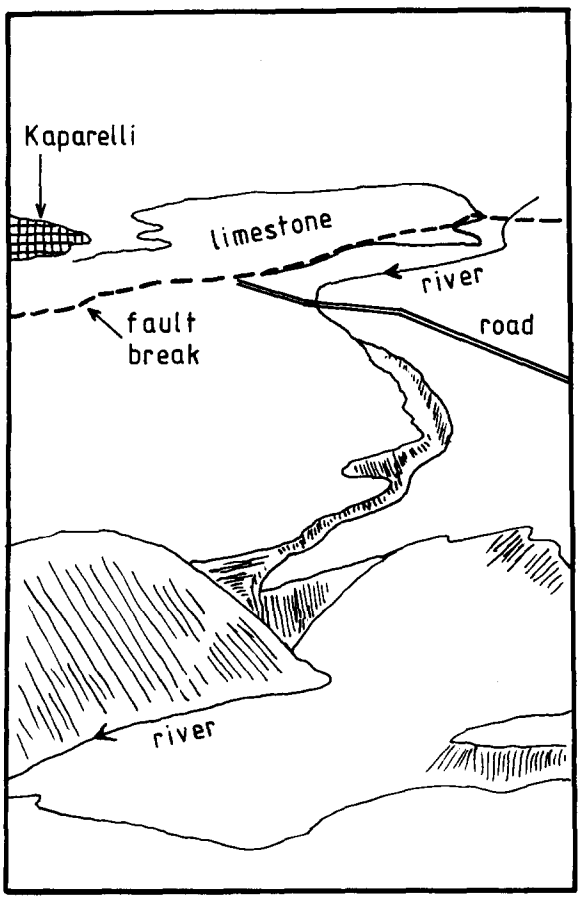

Fig. 8. View looking eastwards up the Livadostros valley towards Platea. Note the undulating erosion surface cut into by the river gorge and the lineation on the right, which is also visible in Fig. 11. The eastern section of the March 4 fault break follows the contact between the limestone and the erosion surface alluvium on the left before crossing the gorge.

Fig. 9. The eastern section of the March 4 fault break south of Kaparelli. Note the 3 m high limestone fault scarp in the background.

Fig. 10. The eastern end of the March 4 fault break, where it leaves the limestone scarp, which continues eastwards, and crosses the valley towards Platea. View looking NW.

Fig. 11. Air photo of the Livadostros valley (see Fig. 6 for location). The 1981 fault breaks follow the limestone-alluvium contact in the eastern (right) part of the picture, and cross the valley at the dissected topography where the gorge starts to widen.

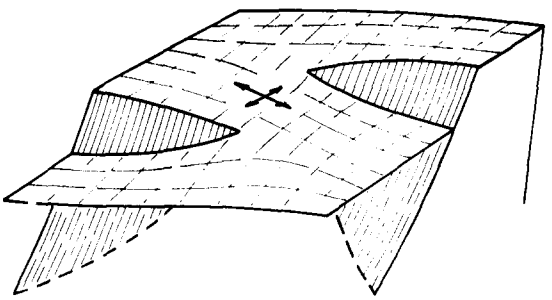

Fig. 12. Cartoon showing the warping of the surface between two offset normal faults, and a component of extension parallel to their strike. This geometry may account for the discontinuous cracking between the two main segments of the March 4 surface breaks, and also for the strike of some of the minor faults at the western end of the Perakora peninsular (Fig. 2) that lie between the postulated offshore fault and the main fault escarpment south of Pision.

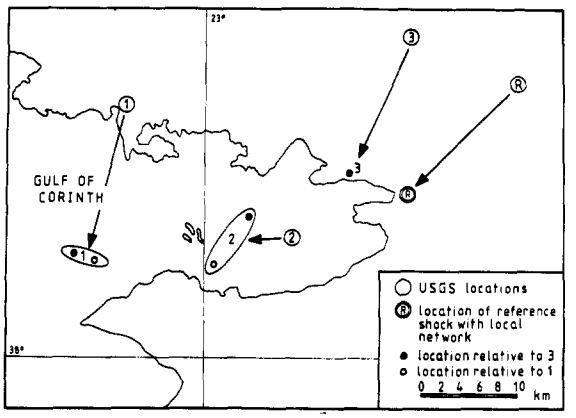

Fig. 13. Epicentre locations. Arrows show the difference between U.S.G.S. and relocated epicentres for the shocks of February 24 (*1*), February 25 (*2*), March 4 (*3*) and March 7 (*R*).

this section are both the regional direction of slip and the more northwesterly azimuth at the western end of the eastern segment. Both this eastern segment and the entire surface break on the southern side of the Gulf appear to have concave ends with slip vectors pointing in towards the centre of curvature. This may be explained as an end effect at the surface if fault motion is finite in lateral extent at depth. On this basis, the western segment of this northern faulting, which does not show these end features, probably continues further west into the Gulf.

4. Epicentral locations

Preliminary locations from the U.S.G.S. are shown in Fig. 13. These are unlikely to be accurate to better than 20 km and so a relative location procedure [8] was used to produce an improved pattern of relative epicentres for the three largest shocks and a fourth, reference shock, which was also accurately located by local seismic stations, and thus allows the pattern to be positioned geographically. This technique has been proved useful by other similar studies [9,10]. The reference shock used was of m_b 5.5 on March 7 (Table 1) and was recorded by eight local stations (Fig. 1) as well as teleseismically.

The relative epicentre pattern was obtained by locating relative to the shock of March 4. This had a greater number of stations reporting to the U.S.G.S. than the first shock of February 24, and has a better station distribution, particularly to the south. Moreover, many stations reported impulsive arrivals for the March 4 shock. These differences affect the quality of the location and are especially important for the reference (March 7) shock, whose location decides the geographical positioning of the epicentre pattern. Stations may only be used in a relative location if they record both shocks. This requirement allows a significantly better station distribution to be used if the reference shock is located relative to the March 4 rather than the February 24 event (Fig. 14). Relocations are shown in Fig. 13. The filled circles are the locations relative to the March 4 shock (*3*) and are positioned using the local epicentre determination for the reference shock of March 7 (*R*). The open circles are locations relative to the first shock of February 24 (*1*) placed geographically assuming the position of the March 4 shock is established by its location relative to the reference (*R*). The difference between the two location patterns is not great, though a reasonable estimate of the epicentral errors must be about 5 km. *1*, *3* and *R* all move about 15 km southwest of their U.S.G.S. locations, though the eastward migration is still

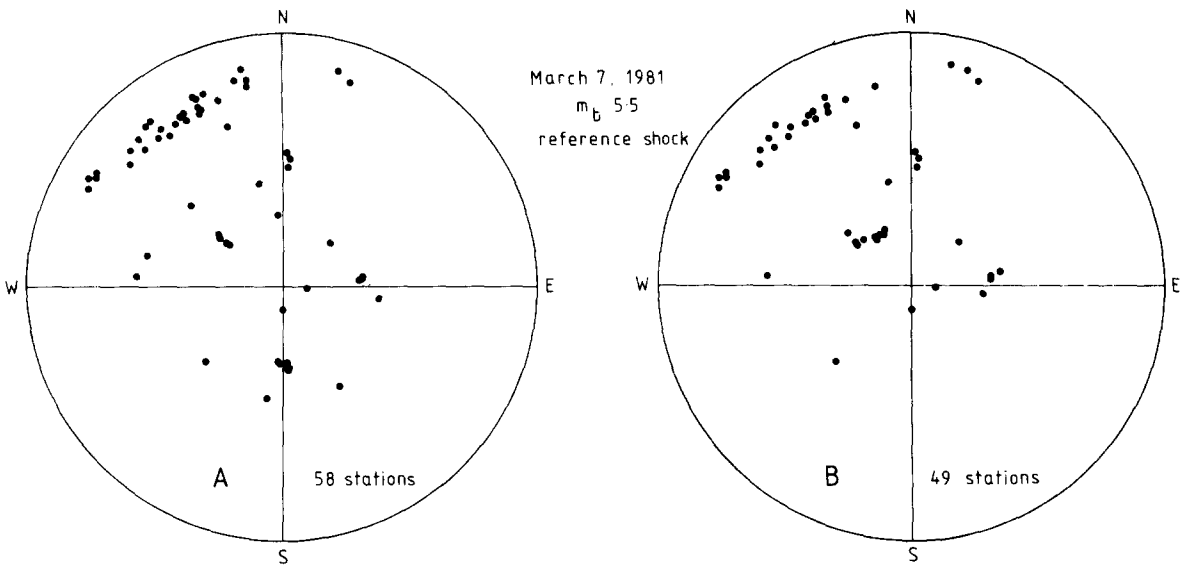

Fig. 14. Lower focal hemisphere plots showing the station distributions used to locate the reference shock (*R* in Fig. 1) relative to the March 4 (A) and the February 24th (B) shocks.

clear. The new locations agree better with the damage reports for shock 1 (discussed later) and put the epicentre of 3 to the south of its southerly dipping fault break. They also suggest that the shock of March 7 (*R*), which caused damage and ground cracks at Porto Germano (Fig. 7) as well as severe shaking at Platea, Erithrea and Vilia (Fig. 1), may be responsible for the cracks on the mountain south of Platea (Fig. 7).

5. Teleseismic observations of the largest shocks

All three largest events produced simple long-period seismograms with first motions and waveforms characteristic of normal faulting. The fault plane solution of the February 24 shock (Fig. 15) is constrained mainly by two compressional readings at IST (NE) and HLW (SE). These require an ESE strike to the northerly dipping nodal plane which is not observed in the faulting seen on land on the south side of the Gulf. The nodal planes have been drawn in Fig. 15 so that they have a slip azimuth on the northerly dipping plane of 010°N. This is consistent with the surface observations in Fig. 2, but clearly the nodal planes are not completely constrained by the first motions alone. Synthetic modelling of the long-period P waveforms was used to constrain focal depth using the program and technique of Langston and Helmberger [11]. The characteristic W shape of the waveforms in Figs. 15, 16 and 17 has been shown by many studies [11–13] to consist of P, pP and sP in the distance range 30–80°, and is very dependent on focal depth. These waveforms may easily be reproduced using a simple source with a mechanism constrained by first motion observations. Uncertainties in the source time function and velocity structure above the source lead to errors in focal depth, assumed to approximate to the depth of rupture initiation, of not much more than ± 2 km [12]. Table 2 lists the time functions and depths of the three largest shocks in Figs. 15, 16 and 17. The shock of February 24 has waveforms which are best modelled with a depth of 10 ± 2 km.

The shock of February 25 (Fig. 10) has a significantly different mechanism, constrained by compressional first motions to the northwest. The northerly dipping plane, which is presumably the fault plane, has a strike with an ENE trend, consistent with that observed at the surface on the

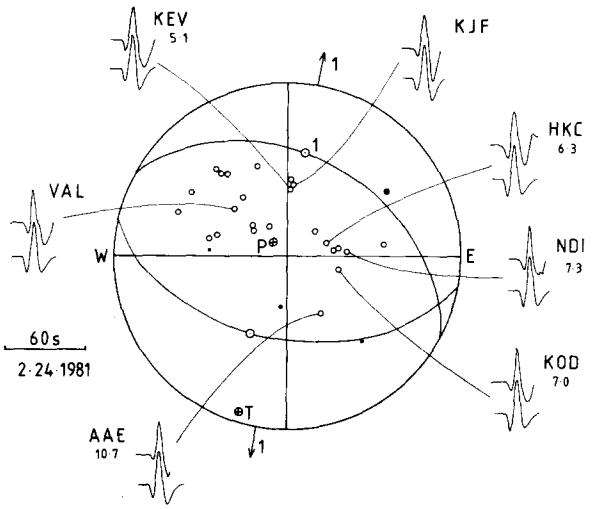

Fig. 15. Lower focal hemisphere and fault plane solution of the February 24 shock. Open circles are dilatations, closed are compressions. All readings are from long-period vertical component WWSSN records. Circles on the nodal planes show slip vectors, and the arrow shows the horizontal projection of the slip vector on the northerly dipping plane. Also shown are observed (top) and synthetic (bottom) long-period P waveforms at selected stations, which were used to estimate focal depth. Beneath each station is a moment value ($\times 10^{25}$ dyne cm).

south side of the Gulf. The southerly dipping nodal plane may be drawn so as to require a slip vector of 010°; again consistent with field observa-

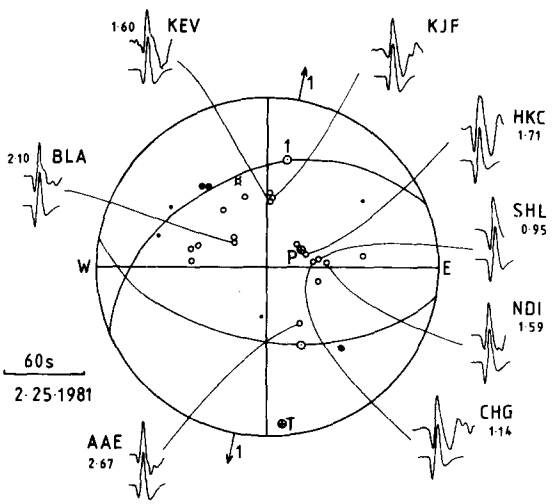

Fig. 16. Fault plane solution and synthetics for the February 25 shock. Nodal first motions are marked with crosses.

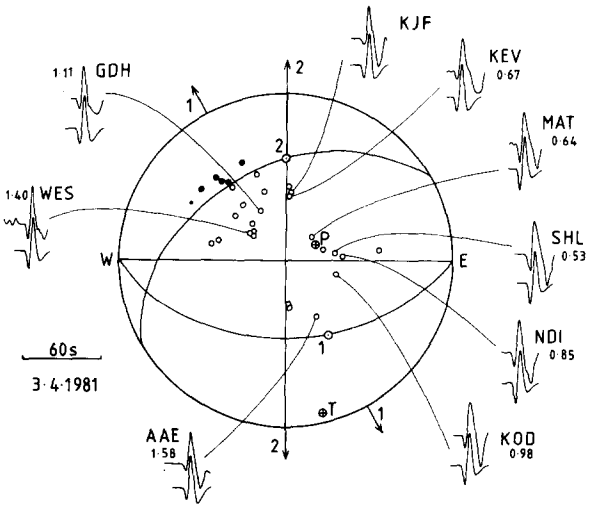

Fig. 17. Fault plane solution and synthetics for the March 4 shock. Horizontal projections of slip vectors are shown for both nodal planes *1* and *2*.

tions. Waveform modelling constrains the depth of this event to 8 ± 2 km.

The shock of March 4 again has a northerly dipping nodal plane which is well constrained by compressions to the northwest (plane 2 in Fig. 17). The surface observations in the Livadostros valley suggest that this is the auxiliary plane. The southerly dipping nodal plane (*1*) can be drawn with the approximately east-west strike of the surface faulting, but the auxiliary plane (*2*) requires a slip vector azimuth in a direction west of north, which is not the slip direction found on either of the main fault segments in Fig. 6. This direction is only found in the confused central area where the faulting crosses the gorge. This will be discussed further in a later section. Waveform modelling, for which it is not necessary to distinguish fault and auxiliary planes, constrains the focal depth to 8 ± 2 km.

The program of Langston and Helmberger [11] calculates the amplitude of ground motion at each station for a particular moment value, and by scaling this with the observed seismogram amplitude a moment value for the earthquake can be found. In Figs. 15–17 the moment at each station is shown, and averages are listed in Table 2. Some stations a little closer than 30°, such as KJF (26°)

TABLE 2

Focal parameters used for generating synthetic waveforms. The source time function is trapezoidal, described by a rise, a plateau and a fall time [11]

	Origin time (GMT)	Strike	Dip	Rake	Depth (km)	$M_0 \times 10^{25}$ (dyne cm)	Time function (seconds)
February 24, 1981	20 53 38.7	300	42	−74	10	7.28	2.0, 3.0, 2.0
February 25, 1981	02 35 53.3	248	42	−115	8	1.68	2.0, 0.0, 2.0
March 4, 1981	21 58 07.5	090	52	−70	8	0.97	2.0, 0.0, 2.0

and VAL (27°) were not used in the averaging because the geometrical spreading factors needed for amplitude estimation are not reliably defined at these distances [11] even though the waveforms have simple shapes. The moment values in Table 2 must be considered uncertain by at least a factor of two, because of both the variation in values between stations and because values of moment deduced from long-period P waves in this manner are often a factor of two or three times smaller than values estimated from 100-second Rayleigh waves for earthquakes in this size range [14–16].

Table 3 lists fault parameters estimated from both teleseismic and surface rupture observations, assuming rupture to a depth of 10 km at a dip of 45° for each fault. If the February 24 shock had no surface break on land, the February 25 event apparently displays more surface faulting than the seismically determined moment suggests. This could be explained by the body wave estimate being too small. Alternatively, both the February 24 and 25 events could have contributed to the southern surface ruptures on land. In this case the combined body wave moment is comparable to that estimated from field data. This is later discussed in more detail.

6. Uplift and subsidence observations

The entire coastline in the eastern part of the Gulf from Kiato to the coast south of Korini was

TABLE 3

A comparison of fault parameters estimated from both teleseismic and field observations for the three largest events. As there are no unequivocal surface observations of the first shock, teleseismic estimates are calculated for a fault length of 15 km and shown in brackets. Surface observations are shown for the second shock assuming it was responsible for all the motion on the southern surface breaks. Parameters are calculated using the relations:

$$M_0 = \mu \mathfrak{M}_0,\ \bar{u} = \mathfrak{M}_0 / A,\ \Delta e = \frac{C\bar{u}}{L},\ \Delta\sigma = \mu\, \Delta e$$

where A is the fault area, L is the shortest fault dimension (10 km in each case), C is a constant of approximately unity, $\mu = 3 \times 10^{11}$ dyne cm and 1 bar $= 10^6$ dyne cm^{-2}. Fault dips are assumed to be 45°. Given the uncertainties in moment and fault dimensions, errors in the teleseismic estimates $\bar{u}$, Δe and $\Delta\sigma$ must be at least a factor of four

	Moment $\mathfrak{M}_0$ ($\times 10^7$ m^3)		Fault length (km)	Fault depth (km)	Mean displacement $\bar{u}$ (m)		Strain drop Δe ($\times 10^{-5}$)		Stress drop $\Delta\sigma$ (bars)	
	seismic	field	field	assumed	seismic	field	seismic	field	seismic	field
February 24, 1981	24.0		(15)	10	(1.15)		(11.5)		(33.6)	
February 25, 1981	5.0	17.0	15	10	0.24	0.8	2.4	8.0	7.0	24
March 4, 1981	3.0	9.9	14	10	0.15	0.5	1.5	5.0	4.5	15

Fig. 18. Uplift of a limestone solution level at Milokopi (Figs. 2 and 3). In the foreground (book) is the trace of the fault break at Milokopi which follows a limestone scarp inland. Uplift is not interrupted by this minor fault.

Fig. 19. A sinking region 2 km east of Skinos, showing a swampy, inundated coastline, behind which is the limestone cliff of the lower of the two major southern escarpments.

examined on shore and by boat for evidence of recent uplift or subsidence. The area south of Kiato and Corinth displays many raised beach terraces up to 150 m high in Neogene and Quaternary deposits. These are discussed in detail by Sebrier [5] and are clear evidence of Quaternary uplift. This uplift continues round the coast as patches of raised beach (Fig. 2) but, more strikingly, as uplifted undercut or solution levels in crystalline limestone (Fig. 18), as far as the point marked *A* (Fig. 2), 2 km north of Milokopi. Between *A* and *B* there is no discernable uplift or subsidence, but from *B* east to Alepohori (*C*) there is clear evidence of a sinking coastline, with a lack of limestone undercut levels, cliffs cut into alluvial fans, and marshy inundation (Fig. 19). From *C* to point *D* more uplift is seen in the form of raised beaches and limestone solution levels, especially in the cliff at *D*. North of *D* and round the entire northern part of the coast in the eastern Gulf is a sinking coastline, with severe inundation at Psatha, limestone solution levels visible below water, and cliffs in alluvial fans.

Of particular interest is the relation between this coastline movement and the faulting. Fig. 2 shows how sinking in the hanging wall changes abruptly to uplift in the footwall as the line of the two large southern escarpments is crossed at *C*. The bathymetry (as seen from helicopter) suggests strongly that at this point the fault goes offshore to join up with another major limestone cliff escarpment on the south side of Psatha bay at D. The cliff at *D* shows clear uplift of solution levels in what is presumably the footwall of a major fault, whereas the whole of Psatha bay is swampy and inundated, and appears to be sinking fast. The other more minor fault systems in Fig. 2, as well as the faults in the Livadostros area, and the numerous minor fault scarps south of Korini, do not, however, appear to have any relation to coastline changes.

Uplift of the footwall in normal faulting is described by numerous authors (e.g. [3,17–20]) and may be modelled elastically in the manner of

Fig. 21. Schematic section of the eastern Gulf of Corinth. (a) shows the topography from south of Corinth to Livadostros with a vertical exaggeration of four. The major faults crossed by the section are marked, and the marine sediments of the Isthmus of Corinth are shown by dark shading. (b) shows the final surface deformation of a fault system that first dropped the sedimented region below sea level by motion on fault *1*, and then raised it by motion on fault *2*. (c) shows the unexaggerated geometry of the faults used in (b) which was produced assuming motions on faults *1*, *2* and *3* of 0.5 km, 1 km and 0.25 km; corresponding roughly to the heights of the scarps in the topographic section (a).

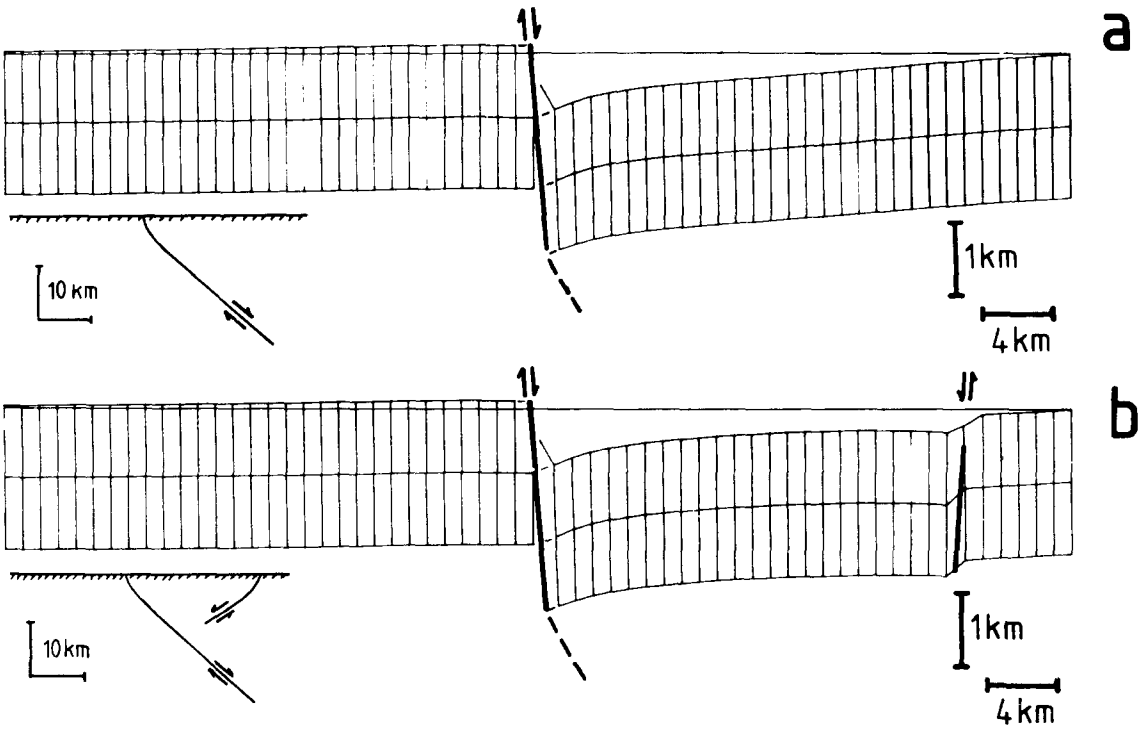

Fig. 20. Surface deformation associated with normal faulting. (a) shows a single listric fault. The footwall uplift is approximately 10% of the downdrop of the hanging wall. (b) shows the same geometry as before but with a small antithetic fault added in the hanging wall. Note that the antithetic fault does not cause net uplift of its own footwall because of the predominant subsidence of the main fault. The main figures are drawn with a vertical exaggeration of four, whereas the insets show the fault geometries to a greater depth with no vertical exaggeration. The listric form of the faults is approximated using three segments in each case, the lowest agreeing with the focal depth and dip estimated teleseismically. The main fault has a displacement of 1 km and the antithetic of 0.25 km on all segments.

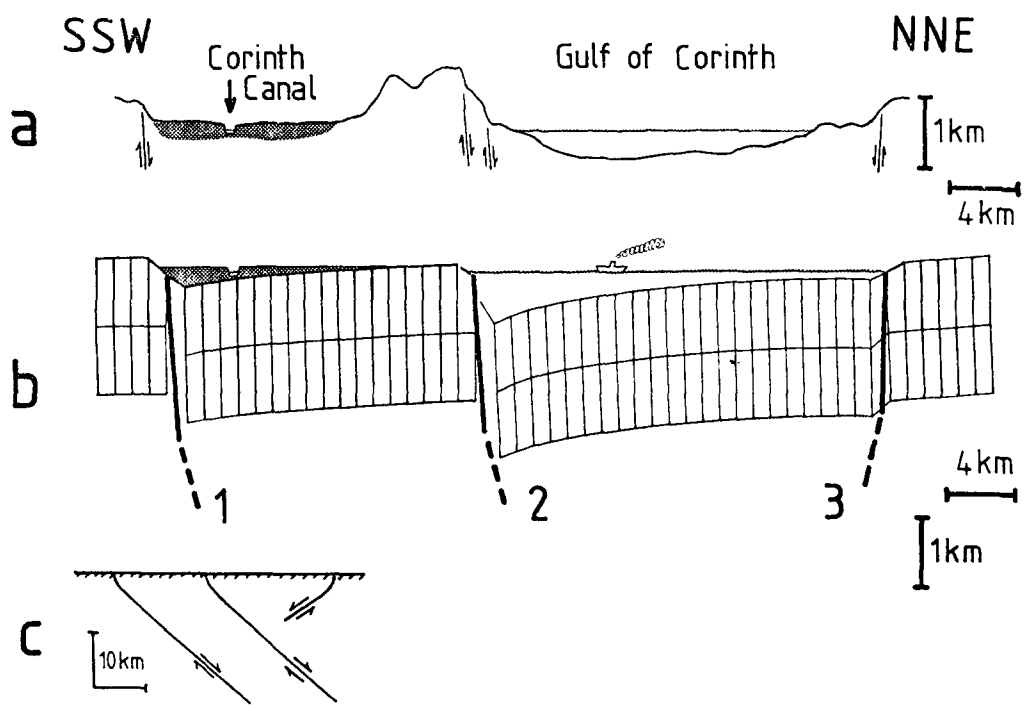

Fig. 21. See p. 392 for explanation.

King and Vita-Finzi [21] as shown in Fig. 20a. This shows that uplift is of the order of 10% of the throw on the fault and extends back into the footwall for distances roughly the order of the fault depth. The fault geometry in Fig. 20 is taken to be consistent with that obtained from the fault plane solutions.

It is thus likely that coastline behaviour between Skinos and Psatha (Figs. 1, 2 and 3) is controlled by movement on the two major southern fault escarpments. We suggest that the minor faults on the southern side of the Gulf, including the surface break at Milokopi, do not affect the coastline because they are much smaller and represent internal deformation in the downthrown hanging wall of the main fault. Such deformation is a geometrical requirement of listric normal faulting and usually causes intense aftershock activity in the hanging wall [9]. There is some evidence for a listric shape to the fault surfaces here, in that all three fault plane solutions have nodal plane dips of 40–50° whereas at the surface the fault dips are nearly vertical. However, the epicentres of February 25 and March 4 are roughly the same distance from the fault outcrop as their depths, and the dips of the surface displacement vectors in the central parts of the fault segments agree reasonably well with the fault plane solutions, suggesting that steepening of the fault plane happens close to the surface. Nevertheless, hanging wall deformation is sufficiently common to be expected in most fault systems.

The marked asymmetry of the Gulf can be explained if the faulting on the north side is antithetic to the major faulting on the south. In this case, the whole northern area is sliding down the major southern fault surfaces with occasional antithetic faults accommodating large internal deformation of the hanging wall (Fig. 20b). No net uplift is then expected in the footwall of the antithetic fault.

7. Discussion of the February 24 shock

Whereas the association of the March 4 shock with the Livadostros faulting and the February 25 shock with the major southern fault escarpments is easy to make, it is less easy to associate the first earthquake of the series, on February 24, with observed surface faulting. It could have occurred on the main southern escarpments but we believe a fault which outcrops underwater and further west was responsible. The evidence for this is:

(1) The fault plane solution requires a strike to the northerly dipping plane (Fig. 15) which is not seen in the main segment of the observed southern surface breaks, but is seen in the bathymetry further west.

(2) The relocated epicentre lies significantly west of the surface breaks, and not down-dip from them.

(3) Local populations at Moulki, Kiato, Prodromou, Thisvi and Korini (Fig. 1) all reported that the greatest shaking occurred in the first shock of the series at 10:53 p.m. local time on February 24. Many could not distinguish the shocks of February 25 and March 4 from other aftershocks. Perakora, Pision and Skinos were badly damaged on both February 24 and 25. However, because the February 24 shock was considerably larger (Table 3) these data are somewhat equivocal.

(4) Local people at Skinos and elsewhere reported a tsunami about 1 m high immediately following the first shock [22], which would be expected from a fault scarp forming underwater. There were no reliable reports of tsunamis from later shocks in which faulting certainly occurred on land. However, tidal waves are known to have occurred in the Gulf of Corinth in the absence of earthquakes, presumably as a result of submarine slumping (N. Ambraseys, personal communication).

(5) The clear uplift of the coast from Kiato to Milokopi implies a major fault offshore.

(6) The bathymetry (Fig. 1) shows a steep escarpment of approximately 500 m high offshore from Kiato and Milokopi. This is comparable to the heights of each of the two major southern escarpments on land, and has the northwest trend of the northerly dipping nodal plane seen in the fault plane solution (Fig. 15). At its eastern end it changes to a northeast trend and dies out. Although a similar trend is seen in the bathymetry on the northern side, this is less steep than the

southern, and movement on this, dipping south, would not produce the observed uplift on the southern shore.

We feel it is likely that the February 24 shock occurred on a fault dipping north associated with the offshore escarpment near Kiato, but this is hard to prove. Aftershock data currently being studied may help considerably. Neither the February 25 nor the March 4 shocks seem to be able to account for all the observed motion on their respective faults (Table 3), though errors are large. This discrepancy may in part be caused by post-seismic creep or motion in aftershocks.

8. Summary and discussion

In summary, the evidence presented here suggests that the February 24 and 25 shocks occurred on major north-dipping faults, the first outcropping underwater and the second running east from Pision. These features are primarily responsible for the bathymetry, topography and coastline uplift and subsidence round the eastern end of the Gulf of Corinth, which is thus a predominantly asymmetric graben, with antithetic faulting on the northern side. Many grabens are probably asymmetric in this way, as pointed out in a recent review by Bally [23]. The pattern of uplift and subsidence shown here bears an uncanny resemblence to that seen in the 1928 earthquake sequence near Plovdiv in Bulgaria [3] in which uplift of 10% (40 cm from 4 m downthrow) occurred in the footwall of a normal fault and the general subsidence of the hanging wall was interrupted by antithetic faulting.

One remaining problem is the discrepancy between the slip vector azimuth on the southerly dipping nodal plane of the March 4 event (Fig. 17) and that observed at the surface. There are various possibilities, since the focal depth of the event indicates that rupture must have initiated close to the projected intersection of the southerly dipping antithetic surface with the northerly dip of the main southern faults. Rupture could have occurred on the main northerly dipping surface and caused the antithetic to move, though the surface breaks more than account for the estimated bodywave moment (Table 3), making it unlikely that there is substantial hidden faulting at depth. Only in the anomalous central section of the surface breaks, where the two main segments are offset, is the azimuth of the fault plane solution slip vector seen. Fault offsets are suspected of being important in controlling rupture initiation and propagation [10,24] and the rupture may have started at depth beneath this offset and been dominated by its direction. However, it is doubtful whether sufficient fault area of this orientation is available for the generation of the observed seismic moment. Neither short nor long-period seismograms help by showing any revealing complications, and further resolution of this matter must await detailed aftershock analysis.

The easterly migration of the seismicity, with the largest shocks separated by roughly their fault dimensions, is most striking. Local people in Platea and Kaparelli reported many aftershocks (foreshocks?) in the week preceding the March 4 event. These were described as shorter and sharper (i.e. closer) than the large shocks of February 24 and 25 which were felt strongly, but with a longer-period character. U.S.G.S. locations do show activity in this part prior to March 4, but it is poorly recorded, and in view of the large mislocations shown in Fig. 13, must await the availability of more arrival time data before reliable relocations are possible.

The fault systems described here effectively drop the erosion surface by Platea (about 300 m high) down to the bottom of the Gulf of Corinth (about 900 m deep) in a series of steps. The dimensions of these fault systems are similar to the en echelon patterns seen in the Bay of Biscay continental margin [25], which is a series of asymmetric grabens forming a sedimentary basin. The eastern part of the Gulf of Corinth thus provides a fine example of the change in geomorphology as normal faulting progresses. Particularly revealing is the destruction of the old erosion surface by Platea as the faulting progresses eastwards. The reactivation of the relatively young fault in the western of the two northern segments rather than the obviously older and larger fault immediately north of the Livadostros river (Figs. 6 and 7) is an example of faulting migrating away from the old scarp into

the hanging wall. This process was observed in the Thessaloniki region [26] and probably also occurred on the south side of the Gulf where the Neogene deposits of the Isthmus of Corinth, through which the canal is cut, have been uplifted as the result of motion on the Kiato and Pision escarpments. Behind Corinth and Ancient Corinth (Fig. 1) is a large normal fault escarpment in limestone [5], which may partly have controlled the deposition of the Neogene and Quaternary sediments, but is probably now responsible for less motion than the escarpments further north. Nonetheless, subsidence of an archeological site at Kechrie, close to this fault and in the hanging wall, may be evidence of some activity. Fig. 21 gives a schematic section across the eastern part of the Gulf showing that the uplift of the Neogene sediments in the Isthmus can be explained if the main fault activity has moved northwards.

Acknowledgements

The fieldwork presented here would not have been possible without the support of the Greek army and General Zervas, to whom we are especially grateful. The army map service kindly provided the air photographs used in Fig. 11. We would like to thank Chris Papanastasiou, Prof. B. Papazachos and the Mayor of Corinth for logistical support. Waverly Person and Russ Needham of NEIC kindly provided arrival time data, and the Royal Society, the Natural Environment Research Council and I.N.A.G. the necessary financial support. This is Cambridge University Department of Earth Sciences contribution No. 188.

References

1 A. Sieberg, Das Korinther Erdbeben von 22 April 1928, Jena. Z. Naturwiss. 64 (1929) 1–20.
2 J. Drakopoulos, G. Leventakis and A. Roussopoulos, Microzonation in the seismic area of Corinth-Loutraki, Ann. Geofis. 31 (1978) 51–96.
3 C.F. Richter, Elementary Seismology (W.F. Freeman, San Francisco, Calif., 1958).
4 D.P. McKenzie, Active tectonics of the Alpine-Himalayan belt: the Aegean Sea and surrounding regions, Geophys. J.R. Astron. Soc. 55 (1978) 217–254.
5 M. Sebrier, Tectonique recente d'une tranversale a l'arc Egeen, Thèse de 3eme cycle, Paris (1977).
6 J.-L. Mercier, E. Carey, H. Phillip and D. Sorel, La neotectonique plio-quaternaire de l'arc Egeen externe et de la mer Egee et ses relations avec seismicite, Bull. Soc. Geol. Fr. 18 (1976) 355–372.
7 J.-L. Mercier, La neotectonique, ses methodes et ses buts. Un example: l'arc Egeen (Mediterranee orientale), Rev. Géogr. Phys. Géol. Dyn. 18 (1976) 323–345.
8 J.A. Jackson and T.J. Fitch, Seismotectonic implications of relocated aftershock sequences in Iran and Turkey, Geophys. J. R. Astron. Soc. 57, (1979) 209–229.
9 C. Soufleris, J.A. Jackson, G.C.P. King, B.C. Papazachos, C. Scholz and C. Spencer, The 1978 earthquake sequence near Thessaloniki (northern Greece), Geophys. J. R. Astron. Soc. (in press).
10 G. Yielding, J.A. Jackson, G.C.P. King, H. Sinvhal, C. Vita-Finzi and R.M. Wood, Relations between surface deformation, fault geometry, seismicity, and rupture propagation characteristics during the El Asnam (Algeria) earthquake of 10 October 1980, Earth Planet. Sci. Lett. 56 (1981) 287–304.
11 C.A. Langston and D.V. Helmberger, A procedure for modelling shallow dislocation sources, Geophys. J. R. Astron. Soc. 42 (1975) 117–130.
12 J.A. Jackson and T.J. Fitch, Basement faulting and the focal depths of the larger earthquakes in the Zagros mountains (Iran), Geophys. J. R. Astron. Soc. 64 (1981) 561–586.
13 C. Soufleris and G.S. Stewart, A source study of the Thessaloniki (N. Greece) 1978 earthquake sequence, Geophys. J. R. Astron. Soc. 67 (1981) 343–358.
14 R. Butler, G.S. Stewart and H. Kanamori, The July 27 1976 Tangshan, China, earthquake—a complex sequence of intraplate events, Bull. Seismol. Soc. Am., 69 (1979) 207–220.
15 J. Cipar, Source processes of the Haicheng, China, earthquake from observations of P and S waveforms, Bull. Seismol. Soc. Am. 69 (1979) 1903–1916.
16 J.E. Ebel, Source processes of the 1965 New Hebrides Islands earthquakes inferred from teleseismic waveforms, Geophys. J. R. Astron. Soc. 63 (1980) 381–403.
17 G. Zandt and T.J. Owens, Crustal flexure associated with normal faulting and implications for seismicity along the Wasatch Front, Utah, Bull. Seismol. Soc. Am. 70 (1980) 1501–1520.
18 W. Thatcher and J.B. Rundle, A model for the earthquake cycle in underthrust zones, J. Geophys. Res. 84 (1979) 5540–5556.
19 J.C. Savage and L.M. Hastie, Surface deformation associated with dip slip faulting, J. Geophys. Res. 71 (1966) 4897–4904.
20 W.B. Myers and W. Hamilton, Deformation accompanying the Hebgen Lake earthquake of August 17, 1959, U.S. Geol. Surv. Prof. Paper, 435 (1964) 55–98.
21 G.C.P. King and C. Vita-Finzi, Active Folding in the Algerian earthquake of 10 October 1980, Nature 292 (1981) 22–26.
22 EOS, Trans. Am. Geophys. Union 62 (1981) 480.

23 A.W. Bally, Musings over Sedimentary basin evolution, Philos. Trans. R. Soc. London (in press).
24 G. Lindh and D.M. Boore, Control of rupture by fault geometry, Bull. Seismol. Soc. Am. 71 (1981) 95–116.
25 O. de Charpal, P. Guennoc, L. Montadert and D.G. Roberts, Rifting, crustal attenuation and subsidence in the Bay of Biscay, Nature 275 (1978) 706–711.
26 J.-L. Mercier, N. Mouyaris, C. Simeakis, T. Roundoyannis and C. Angelidhis, Intraplate deformation: a quantitative study of the faults activated by the 1978 Thessaloniki earthquakes, Nature 278 (1979) 45–48.